SKI Report 2008:05

Research

ULiAS 4 – Experimental validation of a software that models ultrasonic wave propagation through an anisotropic weld

Håkan Wirdelius
Gert Persson
Kenneth Hamberg
Kjell Högberg

2008

ISSN 1104-1374
ISRN SKI-R-08/05-SE

SKI

ULIAS projektet (1997- 2007)

Forskningsprojektet ULIAS (UltraLjudsegenskaper I Austenitiska Svetsar) startade 1997 på intiativ från OKG AB och SKI. Syftet med projektet var att studera och mäta egenskaper hos austenitiska svetsar. Egenskaper som tros ha stor inverkan på ultraljudets utbredning vid en inspektion med ultraljud. SKI:s krav på kvalificering av provningssystem skapade ett nytt behov av information om dessa materialegenskaper och projektet skulle bland annat bidra till ökad överensstämmelse mellan verkliga objekt och de kvalificeringsobjekt som behövdes vid en kvalificering. Projektets målsättning var alltså att införskaffa kunskap om mekaniska komponenters materialstruktur så att överensstämmelse skulle kunna uppnås mellan verkligt objekt och kvalificeringsobjekt. Ett steg på vägen till att erhålla sådan överensstämmelse var att ta fram data till existerade datormodeller samt införskaffa kunskap om hur sådana modeller kan förfinas. Man ville också kunna studera och koppla krav på svetsning till objektets materialstruktur för att i slutändan få ökad förståelse i provningssituationen och ökad provningseffektivitet.

Svårigheten med att prova austenitiska svetsar med ultraljud beror bland annat på att kristallerna stelnar dendritiskt och ger ett mönster av pelarliknande kristaller i storleksordningen 1 mm. Materialet blir således elastiskt anisotropt (riktningsvarierande ljudhastigheter) vilket resulterar i ljudavböjning och divergens av ljudfältet. Därtill ger effekter såsom modomvandling i dendritgränserna, dämpning och brus i den mottagna signalen. Fenomen som dessa är svåra att rekonstruera utan matematiska modeller och projektet avsåg därför att möjliggöra modellering av liknande material..

Projektet initierades av SKI tillsammans med OKG men projektet har under åren drivits gemensamt mellan SKI och samtliga svenska tillståndshavare OKG, RAB, FKA och BKAB som också tillsammans med SKI finansierat projektet. SQC Swedish Qualification Center har medverkat som expert, beställare och utförare av vissa moment i det sista delprojektet. Uppdragstagarna har genom åren varit ABB TRC AB (sedermera Wesdyne TRC), Force Technology, SQC och Chalmers (avdelning för avancerad oförstörande provning).

ULIAS del 1

ULIAS projektet inleddes med en litteraturstudie [1] som kom fram till följande slutsatser som är citat ur slutrapporten från ULIAS del 1 [2],

- Ett grundmaterial med slumpvis orienterade likaxliga korn påverkar inte kristallorienteringen i svetsen, utan den styrs helt av betingelserna under svetsning. Grundmaterialets kristallstorlek är dock av betydelse för pelarkristallernas bredd
- Pelarkristallernas längd bestäms av stelnings- och värmeledningsförhållanden
- Vid flersträngssvetsning är underliggande svetssträngars kristallriktning av stor betydelse . Normalt sker tillväxt av pelarkristaller på underliggande strängs primära dendritarmar. Avviker värmeflödet mycket från riktningen hos underliggande strängs pelarkristaller sker tillväxt på de sekundära dendritarmarna
- Pelarkristallernas lutning i framföringsriktningen är tämligen konstant för olika framföringshastigheter. En minskning från 14° till 9° noterades då framföringshastigheten ökades med en faktor 4. Långsammare hastighet ger alltså en större lutningsvinkel hos pelarkristallerna
- Svetsläget är en mycket viktig parameter för riktningen hos pelarkristallerna. Ett antal typfall finns för cladding utförd i olika svetslägen.

Inom del 1 gjordes dessutom en inventering av relevanta objekt i system 313, 326, 321 och 312 i två av reaktorerna i Oskarshamn [3]. Inventeringen resulterade i en specifikation av 11 st testblock för vidare studier [4].

ULIAS del 2

Inom ULIAS del 2 tillverkades de 11 testblock som föreslagits i del 1 [5]. Testblocken användes till undersökningar av metoder för att kartlägga elasticitetskonstanter i materialen. Projektet producerade tre rapporter:

- Metodik för testblockstillverkning för att kunna bestämma elasticitetskonstanterna i materialen i fråga [6]
- Metodbeskrivning för hur elasticitetskonstanterna kan bestämmas med ultraljud [7]
- Metallurgisk undersökning av testblocken [8]

ULIAS del 3

Inom ULIAS del 3 tillverkades nya testblock för att kunna gå vidare med tillämpning av den metod som föreslogs i ULIAS del 2. Uppmätningar av ljudhastigheterna och dämpningen gjordes i de tre planen. Bestämning av konstanterna C_{11}, C_{22} och C_{33} (delar av den matris som beskriver elastisitetsmodulen) gjordes för 8 svetsar [9]. För att få fullständig information om elasticitetskonstanterna behövdes ytterligare mätningar göras.

Ytterligare en litteratursökning gjordes och resterande konstanter kunde bestämmas med hjälp av information från andra projekt för materialet Inconel 182 [10].

ULIAS del 4

I del 4 som rapporteras i denna SKI rapport modelleras strukturen för austenitiska svetsar med uppdelning av svetsområdet i delområden, som då motsvarar grupperingar av korn (dendriter). Den praktiska delen av projektet utfördes av SQC Swedish Qualification Center i samarbete med Chalmers. Syftet med den praktiska delen som utgör provningen av verkliga objekt, med känd materialstruktur, är här att kunna jämföra experimentella och beräknade data.

Sammanfattning ur ett SKI perspektiv

Projektet visar att problemet med att modellera och beskriva dendritorienteringen i svetsar samt hur provning med ultraljud påverkas av detta är komplext och delvis individuell för varje svets. Mycket ny och viktig information har framkommit och det finns idag i och med detta projekt en förståelse och ett angreppssätt för hur modeller kan utformas för att ta hand om detta. Projektet har också visat hur dendriter kan påverka ultraljudsprovning.

För framtiden och fortsatt arbetet ser SKI att modellen kan förfinas ytterligare och valideras med mer experiment och studier i verklig miljö.

Referenser

[1] Söderman L., Litteraturstudie – Textur i austenistiska svetsar, ABB TRC AB Rapport R-T97-88, 1997

[2] Ultraljudegenskaper i austenitiska svetsar, Forskningsprojekt del 1, Slutrapport, R-T98-03, 1998,01-12, ABB Tekniska Röntgenscentralen, TRC
[3] Österberg E., Inventering av objekt, ABB TRC AB Rapport R-T97-108, 1997.
[4] Österberg E., Specifikation av studier, ABB TRC AB Rapport R-T97-113, 1997
[5] Ultrasonic Properties in austenitic welds, ULAS Task 2 – Final Report, Force Institute, May 26, 2000.
[6] P. Krarup, S Halkjaer. Ultrasonic Parameters in Austenitic Weldings, ULIAS Task 2 – Progress report 1. FORCE Institute, July 1999
[7] S.A Nielsen. Ultrasonic Parameters in Austenitic Weldings, ULIAS Task 2 – Progress report 2. FORCE Institute, September 1999

[8] S Halkjaer. Ultrasonic Parameters in Austenitic Weldings, ULIAS Task 2 – Progress report 3. FORCE Institute, May 2000
[9] Ultrasonic Parameters in Austenitic Weldings, ULIAS Task 3 – Final Report. FORCE Institute, May 2000
[10] Collet, N. J. & Hawker, B., “Measurement of elastic constants for Inconel 182 weld material”, Int. Comm. , IVC/RTID/MOD/RAY-1, Culham (1998

SKI Report 2008:05

Research

ULiAS 4 – Experimental validation of a software that models ultrasonic wave propagation through an anisotropic weld

Håkan Wirdelius
Gert Persson
Kenneth Hamberg[1]
Kjell Högberg[2]

1
SCeNDT
Chalmers Univ. Of Tech.
SE-412 96 Göteborg

2
SQC Kvalificeringscentrum AB
Box 519
SE-183 25 Täby

2008

Table of content

Summary

New and stronger demands on reliability of used NDE/ NDT procedures and methods have evolved in Europe during the last decade. In order to elaborate these procedures, efforts have to be taken towards the development of mathematical models of applied NDT methods. Modelling of ultrasonic non-destructive testing is useful for a number of reasons, e.g. physical understanding, parametric studies, and the qualification of procedures and personnel. An important issue regarding all models is the validation, i.e. securing that the results of the model and the corresponding computer programs are correct. This can be accomplished by comparisons with other models, but ultimately by comparisons with experiments. In this study a numerical model and experimental results are compared and the work has been performed in collaboration with SQC Kvalificeringscentrum AB.

Four different welds have been investigated to give basic data to a mathematical model that describes the ultra sonic wave paths through the welds in these materials. The welds are made in austenitic stainless steel (type 18-8) and in Inconel 182. Two cuts outs are made in each weld, one longitudinal and one transversal cut across the welds, in order to determine the material orientation.

In the numerical model the incident field, described by rays, is given by a P wave probe model. The ray tracing technique is based on geometrical optics and a 2D algorithm has been developed. The model of the weld is based on a relatively primitive assumption of the grain structure for a V-butt weld. The columnar structure of austenitic welds is here modelled as a weld where each sub region corresponds to a grain group. The response of the receiver is calculated according to Auld's reciprocity principle. UT data collection was performed by SQC according to guidelines given from Chalmers. The purpose to collect data from real inspection objects with known material structure is to compare experimental data with theoretically calculated values.

The miroscope investigation shows a solidification pattern with a growth of columnar grains (dendrites) that is guided by the thermal gradient due to the welding procedure. A difference in coarseness can be seen depending of the welding procedure. Many weld runs gives a coarser dendritic pattern. The numerical calculations visualizes the ray tracing through the sub regions and produces both a line scan and a C-scan. Comparison with the experimental results shows that it is obvious that the anistropic behaviour varies along the welding direction.

This then indicating that the assumption, that the weld could be considered as transversely anisotropic material in all, did not match with the reality. In order to validate the degree of variation a number of simulations of the same situation was generated with a random variation of the dendrite orientation. These were then combined into a C-scan which made it possible to make a qualitative comparison with the experimental data.

Sammanfattning

Nya och starkare krav på tillförlitlighet för OFP metoder och procedurer, har växt fram i Europa under den senaste tioårsperioden. För att möta dessa krav har stora insatser gjorts inom områden som berör matematisk modellering av tillämpad OFP. Matematisk modellering av OFP med till exempel ultraljud är användbart ur flera aspekter, ökad fysikalisk förståelse, vid parameterstudier och för kvalificering av personal och procedurer. För all matematisk modellering är validering en mycket viktig fråga, dvs att säkerställa att beräknade resultat överensstämmer med resultat från andra modeller och med praktisk provning. I föreliggande arbete jämförs resultat från en matematisk modell med praktisk provning där arbetet utförts i samarbete med SQC Kvalificeringscentrum AB.

Fyra olika svetsar har undersökts för att ge indata till den matematiska modellen, vars syfte är att beskriva hur ultraljudet utbreder sig i den värmepåverkade sonen. Svetsarna är utförda i austenitiskt rostfritt material (typ 18-8) och i Inconel 182. För att bestämma materialorientering har det gjorts två snitt i vardera svets, ett längs och ett tvärs svetsriktningen..

I den numeriska modellen ges det infallande fältet av en P-vågs probe. Modellen bygger på en 2D strålgångsapproximation och det har tagits fram en metod för att beräkna strålgången. Modellen av svetsarna bygger på en relativt enkel modell för korngränser. Strukturen för austenitiska svetsar modelleras här med uppdelning av svetsområdet i delområden, som då motsvarar grupperingar av korn (dendriter). Signalsvaret i den numeriska modellen beräknas mha Auld's reciprocitetsprincip. Den praktiska provningen utfördes av SQC efter riktlinjer från Chalmers. Syftet med provningen av verkliga objekt, med känd materialstruktur, är här att kunna jämföra experimentella och beräknade data.

Undersökningen med mikroskop visar ett stelningsmönster där tillväxten av dendriter sker längs den termiska gradienten som uppkommer vid svetsning. Beroende på hur svetsen utförts finns en skillnad i stelningsmönstret. Vid upprepad svetsning fås ett kraftigare dendritiskt mönster. De numeriska resultaten presenteras dels som strålgångsväg genom svetsens delområden och dels som linje-scan och C-scan. Jämförelse med experimentella resultat visar att det anisotropa beteendet varierar längs svetsens utbredning.

Den sålunda antagna transversella anisotropin är således bara till viss del överensstämmande med verkligheten. För att möjliggöra en jämförelse av graden av variation föreskrevs en slumpmässig variation från ursprungsläget av respektive delvolyms dendritorientering. Ett antal linje-scan sammanfogades till ett C-scan som kunde jämföras med de experimentellt uppmätta. Härigenom gick det att kvantifiera graden av avvikelse från en homogen transversell anisotropi med avseende på svetstyp.

Introduction

Due to new and stronger demands on reliability of NDE/NDT procedures and methods used for in-service inspection in nuclear plants, different demands on qualification of the technique has evolved in Europe during the last decade. In Sweden the qualification that emerged incorporated qualification of used system (i.e. technique, corresponding procedure and personnel). To qualify the procedures extensive experimental work on test blocks is normally required. An infinite number of variables and possibilities have to be reduced into a limited group of statistically relevant NDT situations. Despite the fact that the proposed qualification procedure with test pieces is very expensive it also tends to introduce a number of possible misalignments between the actual NDT situation that is to be performed and the proposed experimental simulation. Also new demands on production optimization and light weight products require new improved techniques to ensure the product quality within conventional industries. Several techniques are used today for non-destructive inspection of components. Automatic as well as manual inspection procedures prerequisite knowledge of the capability to detect, characterise and size defects in specific objects. The capability depends on the geometry of inspected object, what kind of material combination it is composed of and what kind of defect that is addressed. This also demands further development of techniques for inspection of welds and areas with anisotropic behaviour.

Some limited efforts were undertaken more than ten years ago to compare and evaluate some models and corresponding computer programs within the PISC 3 project, see Lakestani [1992). More recently, benchmarking projects have been initiated by the World Federation of NDE Centers (http://www.wfndec.org), and some of these efforts have been reported at the last three conferences in the yearly series Review of Progress in Quantitative Nondestructive Evaluation (Boström [2005], Diligent et al. [2005], Schmerr [2005], Song [2005] and Spies [2005]). Experiments have been conducted on some simple defects, side-drilled holes, flat-bottomed holes, and spheres, in simple immersion testing with unfocussed and focussed probes. These results are made public so that models can be compared with the experiments.

In-service inspection of components that includes welds in austenitic stainless steel and Inconel metal has revealed systematic faults that are due to unpredictable paths of the ultrasound in the welded material. These welds exhibit not only highly anisotropic behaviour but also involve inhomogeneous ultrasonic properties. This is caused by the solidification process and the orientation of the dendrites (i.e. large grain structures) is governed by the temperature gradient in the cooling process. This document describes the fourth part of a project, ULiAS-Ulrasonic properties of austentic weldings , with the overall purpose to give detailed description of these kind welds in order to enable mathematical modelling of the same (Söderman [1997], Österberg [1997], Eriksson [1998], Nielsen [1999], Nielsen [2000], Halkjear [2000] and Nielsen [2002]).

A thorough validated model has the ability to be an alternative or a complement to the experimental work in order to reduce the extensive cost that is associated with the previous procedures. An interesting notation is though that these validations are often performed against very simplified and not thoroughly validated fabricated defects (e.g. EDM notches) with the echo dynamics (i.e. in the ultrasonic NDT case) used as the measurement of its credibility. First, such a model should provide a solution to the forward problem, that is, a quantitative analysis of the probe response to defects of all types. Second, the model should be formulated so as to facilitate the development of solutions to the inverse problem.

In this work four different welds have been investigated by microscope to give basic data of the material orientation to a mathematical model that describes how ultra sonic waves pass through the welds in these materials. The welds are made in austenitic stainless steel (type 18-8) and in Inconel 182. Two cuts are made in each weld, one longitudinal and one transversal cut across the welds.

In the numerical model the incident field, described by rays, is given by a P wave probe model. The ray tracing technique is based on geometrical optics and a 2D algorithm has been developed. The model of the weld is based on a relatively primitive assumption of the grain structure for a V-butt weld. The columnar structure of austenitic welds is here modelled as a weld where each sub region corresponds to a grain group. The response of the receiver is calculated according to Auld's reciprocity principle (Auld [1979]).

UT data collection was performed by SQC according to guidelines given from Chalmers. The purpose to collect data from real inspection objects with known material structure is to compare experimental data with theoretically calculated values.

Microscope investigation.

Background

The welds have been investigated to give basic data to a mathematical model that describes how ultra sonic waves pass through the welds in these materials. All welds have been investigated in a previous project, here are only four different welds analysed. They are designated B27 and A18 in austenitic stainless steel (type 18-8) and C20 and D20 in Inconel 182. These names were given to the welds in the earlier project. The aim of the investigation is to map out the dendrite orientation and shape in the weld.

Materials samples

Two cuts are made in each weld one longitudinal and one transversal cut across the welds. These directions are shown in the figure below.

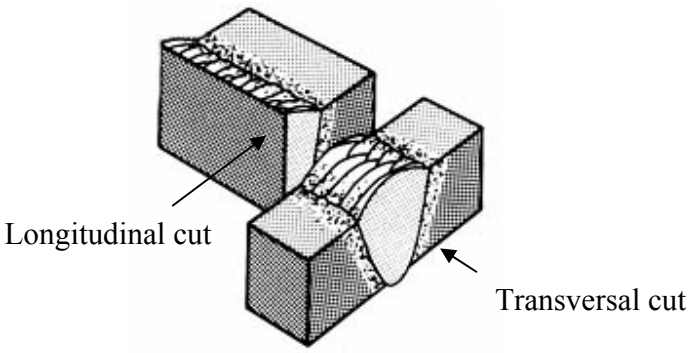

Figure 1: Cuts in the weld.

Geometrically there is a great difference between the two austenitic samples. Sample A18 is considerably thinner than sample B27. Both welds are prepared as U groove before welding. The difference in size implies a great difference in the number of layers needed to fill the U-groove. A18 have 16 layers and in sample B27 the number is 24. Visual inspection of the etched welds shows a macroscopic solidification pattern that is similar in both the austenitic welds and in Inconel. The samples are etch with Marble's enchant (50 ml HCl, 10 g $CuSO_4$ and 50 ml aqua dest.)

While looking at the dendrite structure a similar solidification process emerge. The thermal gradient directs the dendrite growth. At the fusion line the direction is horizontal while at the centre of the weld they are almost vertical. The greatest distance between two weld beads is 2, 5-3 mm, thus the dendrite lengths in the weld must be multiples of this length.

Sample B27.

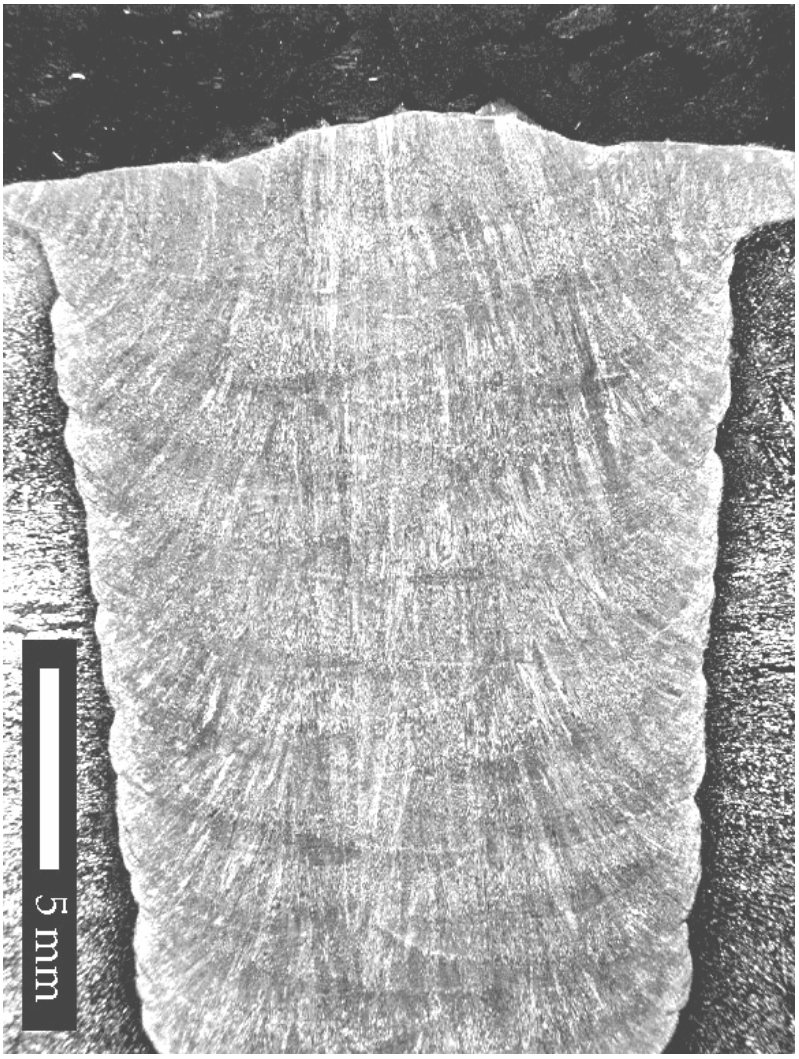

Figure 2: Sample B27, transverse cut.

In figure 2 a macroscopic dendrite pattern fade in quite clearly. At the centre the dendrite arms are as longest and directed more or less vertical. At the fusion line the dendrites follow the thermal gradient which gives and angel of approximately 30-40 degrees compared to the sheet material. Coarser dendrite seems to grow independently of the next weld pass. These coarser dendrites are clearly visible when the sectioned and polished weld is visually inspected. Despite this fact the different weld passes are clearly visible both in figure 2 and 3.

At the fusion line all classical details in a solidificated weld are present. Directly in connection to the fusion line small equiaxed grains are noticeable. Some of these grains develop into a columnar shape they seem to coarsen rapidly both in length and width. Area 1 in figure 3 displays the finer detailed microstructure at the fusion line. The dotted line represents an approximate borderline between two weld passes. If we consider the

boarder line between two weld passes some dendrites seems to grow independently of the new weld pass. Some dendrites do also nucleate at the growing dendrite's surface.

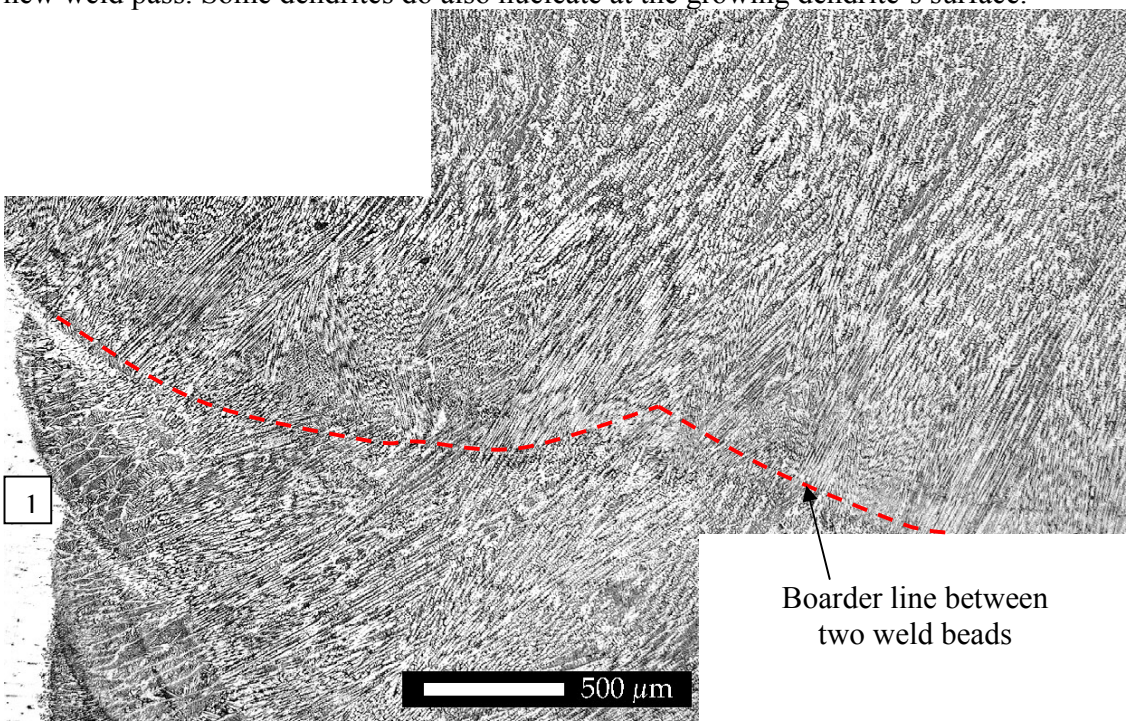

Figure 3: Normal change of the dendrites appearance and orientation

At certain other transitions between two passes local disturbances affect the microstructure. Examples of such disturbances are displayed in figure 4. The reason for these disturbances might bee the welders practice, disturbances in the nucleation condition of the melt, disturbances in the local thermal gradient. In these areas the reflection of the propagation sound wave ought to be altered locally.

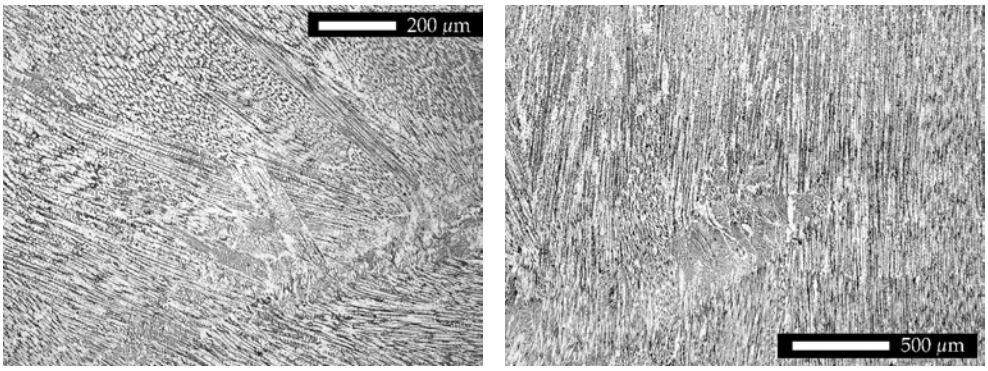

Figure 4: Examples of micro structural disturbance that might affect the scattering of propagating sound wave.

In figure 4 (to the left) some smaller dendrites seems to grow independently of the main growth direction. To the right is another example displayed here traces of unfused part of a weld. These remains are probably due to the welder.

Examples of areas where dendrites grow from the previous weld pass into the new one can bee seen in figure 5. The coarser columnar grains in the first weld pass is partially melted and re solidified by the new weld and the grains continue to grow into the new melt. This time they are finer due to a higher solidification rate. This microstructural appearance ought to disturb a propagation sound wave locally.

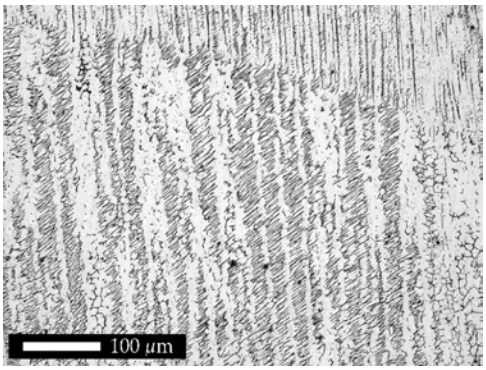

Figure 5: The transition between two weld passes.

If the size of the dendrites is to be put as a number the definition of dendrite is a problem. Figure 6 defines the problem. Here some dendrites displayed and as one can see the dendrite in area A has the same orientation as in area B. The question is if it is the same dendrite. Some other dendrites grow partly in to the new weld pass as seen in the figure. Both the boarder between dendrites and weld pass are marked with red lines. The boarder between the passes is dotted. To state a length of the dendrite is therefore a problem of defining where the dendrite starts to grow and where it stops.

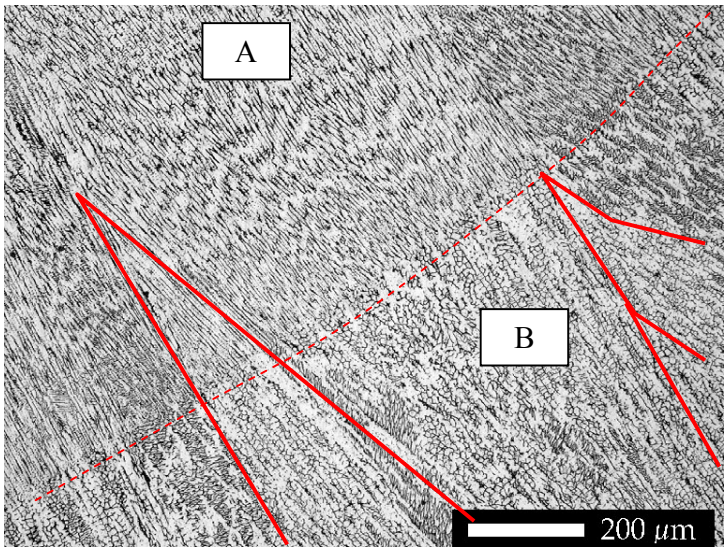

Figure 6: A boarder line between two welds is displayed. A read line enhances the boarder line.

Sample A18

The biggest dendrites are seen in the centre of the weld but the size is change due to the magnification in the microscope. At higher magnifications it is apparent the dendrite consists of different areas with slightly different orientations and appearances. This behaviour can also bee seen in sample B27. Figure 7 shows the macroscopic pattern in test coupon A18. It's evident from the solidification pattern that very small and equiaxed grains are located close to the fusion line and that the dendrites grow depending on the heat that is introduced by the next weald bead. This heat will direct the dendrites but also act as a nucleation site for next grains that will grow in a columnar fusion. Figure 7 shows clearly that orientation change from the middle of the weld and closer to the fusion line.

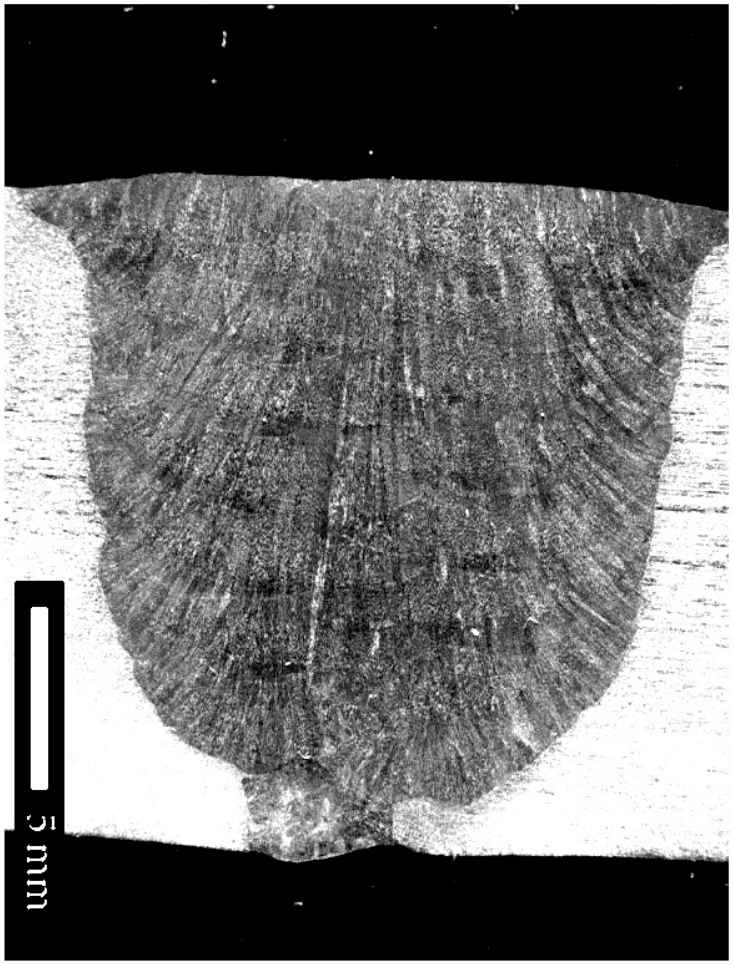

Figure 7: Weld A18, perpendicular to the welding direction.

Broadly the dendrites in weld A 18 show the same behaviour as depicted previously in weld B27, figure 8 below displays a small area of weld 18. It shows an example of dendrites passes the boarder between different layers without any problems. It also shows that other grains will clearly stop at the new fusion line the new weld pass creates in the same manner that is shown in weld B27. The microstructure is developed with Kallings etchant.

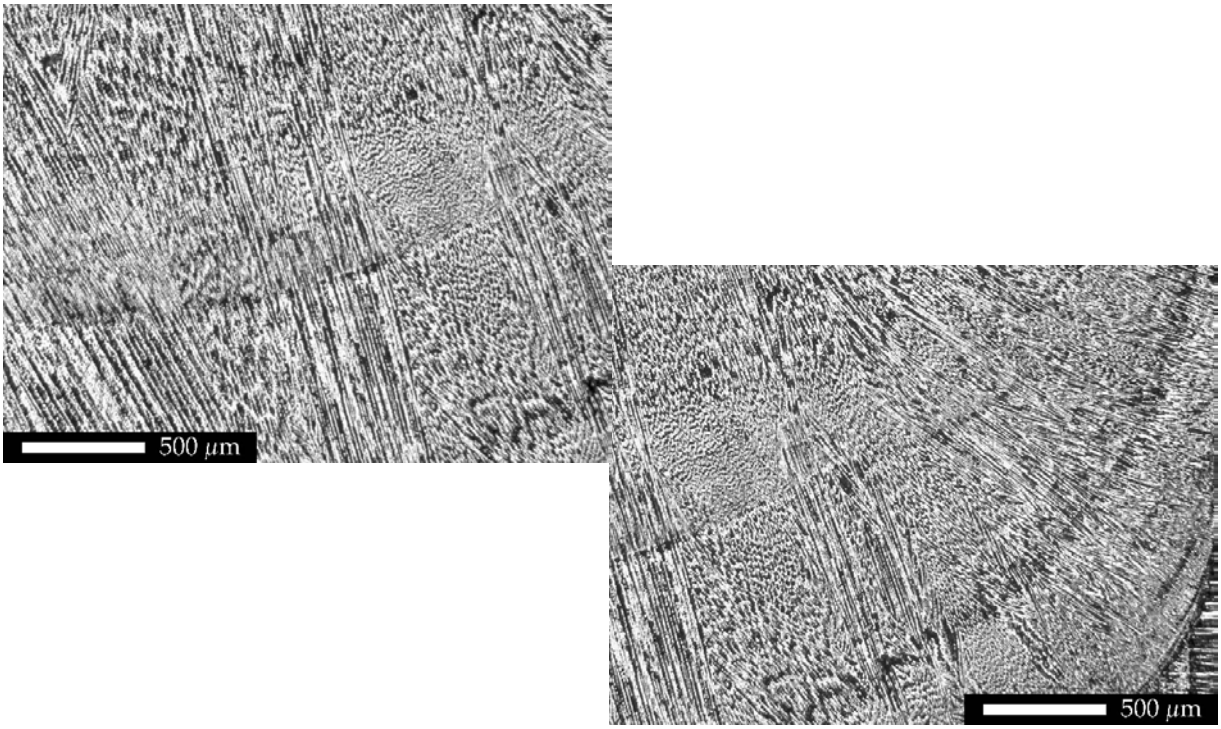

Figure 8: Dendrites in weld A18, the material is a austenitic 18-8 steel.

Inconel 182

The plates are of the same thickness as sample A18 and the grooves are U-shaped. The width of the joint is wider. Each run consists of three weld beads parallel to each other except for the firsts root layer and the next two runs. In sample D 20 and C 20 each weld consists of 19 respectively 23 weld beads. Etchant used is Kallings (40 ml HCl, 50 ml aqua dest. and 2 g $CuCl_2$)

Visual inspection of the two welds shows that the microstructure is a bit finer (smaller) compare to the austenitic steel welds. Each weld bead seems to have its original solidification pattern more or less intact.

Sample D20

Figure 9 indicates the macroscopic structure of the weld. Reason for why the base material takes etching differently is that the plates in the joint are ordinary low alloyed steel and one is made of Income.

In sample D20 the dendrites follow the same pattern as in the austenitic samples. The difference is that the dendrites are smaller. Macroscopically the dendrite pattern (the columnar grains) seems to be less clear compared to sample B27. This is obvious even with a naked eye. Figure 10 shows an area in higher magnification. Here some of the dendrite grows across the local fusion line while others stop at the local boarder line. An estimate with the eye is that 50% passes the new local fusion line. The remaining

columnar grains passes the local fusion line but stops after a short distance and new grains nucleate and starts to grow.

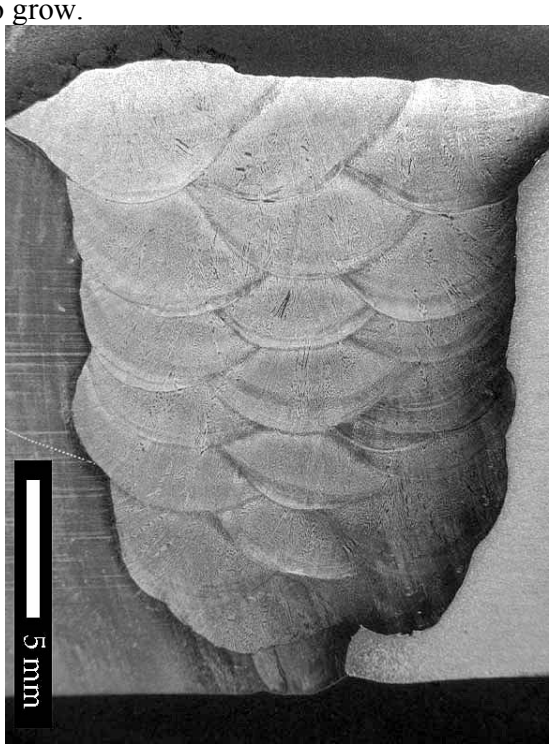

Figure 9: D20 perpendicular to the welding direction.

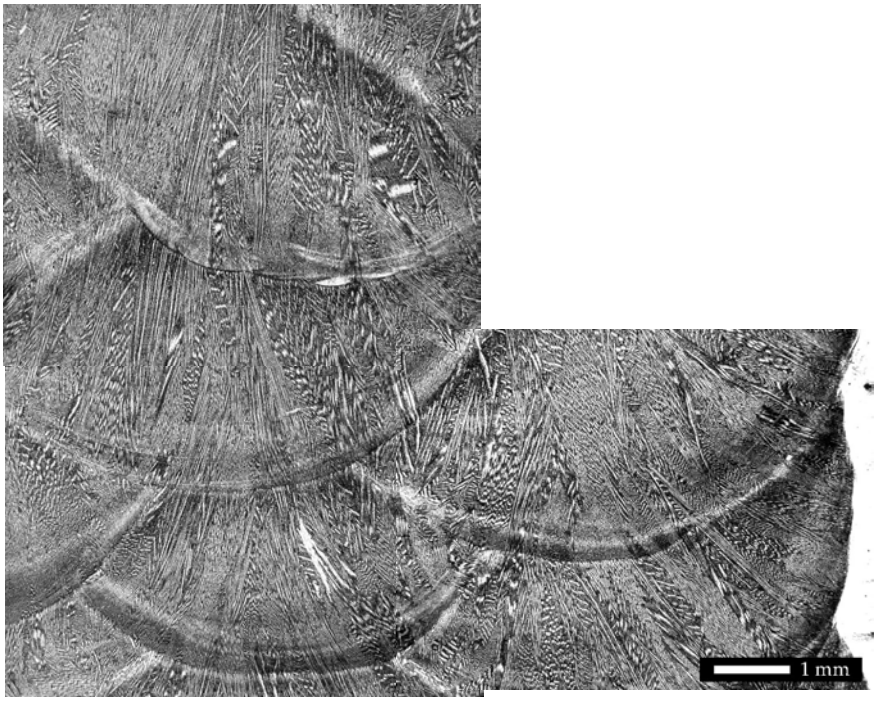

Figure 10: Weld D20 in higher magnification

Sample C20

Weld C20 shows an identical microstructure compared to weld D20. To the left on the figure a shadow appear. This shadow has nothing to do with the microstructure; it's an effect of the etching procedure.

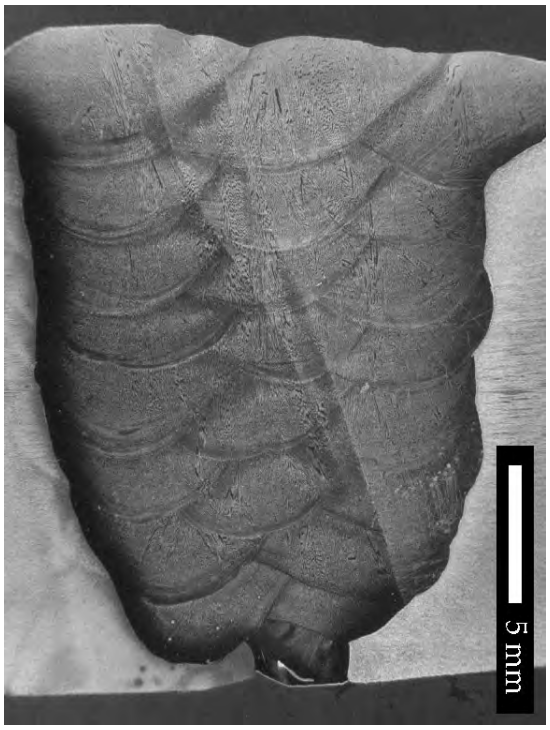

Figure 11: The macroscopic dendrite structure in sample has appearance comparable to weld D20.

Microstructure parallel to the welding direction.

All samples that are investigated show a similar structure. All grains are directed vertical.

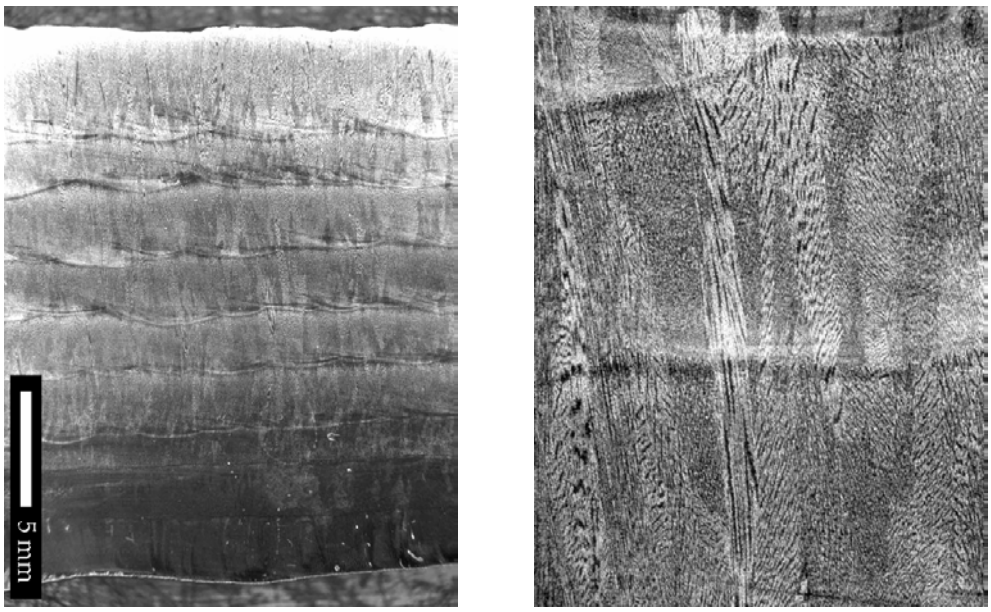

Figure 12: The macroscopic dendrite structure in sample C20 (left) and D20 parallel to welding direction.

Weld C20 and D20 might serve as an example on the grain orientation. All different weld beads are clearly visible as local

Conclusions

- In all four welds a solidification pattern is emerging that show a growth of columnar grains (dendrites) that is guided by the thermal gradient due to the welding procedure. A difference in coarseness can be seen depending of the welding procedure. Many weld runs gives a coarser dendritic pattern
- The dendrites in all samples is affected by the sequence the different weld runs are lied. Some of the dendrites continue to grow on the other side of the local fusion line while other stop at the boarder line.
- In the austenitic material there are local disturbances that might affect the sound wave, see figure 4 and 5.
- In the Inconell welds the dendrites are smaller and they seems to bee more affected by the order of the weld procedure, see figure 10.
- A number of the size of the dendrites is hard to give when it is hard to define the dendrite, see figure 6 and 8.

The ultrasonic model

The probe model

The incident field, described by rays, is given by a P wave probe model developed by Liu and Wirdelius [2006]. In this model the wave traveling in an elastic half space is generated by the pressure created by the probe due to the traction distribution on the surface. In the frequency domain a plane P-wave then, according to fig. ***x1*** , can be expressed as

$$\tilde{\mathbf{u}}_P = A(\sin\gamma\ \mathbf{e}_1 + \cos\gamma\ \mathbf{e}_3)e^{ik_P(\sin\gamma\ x_1 + \cos\gamma\ x_3)}$$

where A is the amplitude and k_P the wave number.

Here the surface under the probe is divided in several sub-areas, each segment is acting as an individual transmitter. The Helmholtz equation

$$\nabla^2\varphi = \frac{1}{c_p^2}\ddot{\varphi}$$

$$\nabla^2\psi = \frac{1}{c_p^2}\ddot{\psi}$$

is solved in the Fourier transform plane and when inverse transforming the expressions is evaluated with the stationary phase method.
Stationary phase calculations will also give the far-field approximation. figure 13 shows the amplitude distribution beneath the boundary conditions that models the probe. One should note that mode conversion is not included

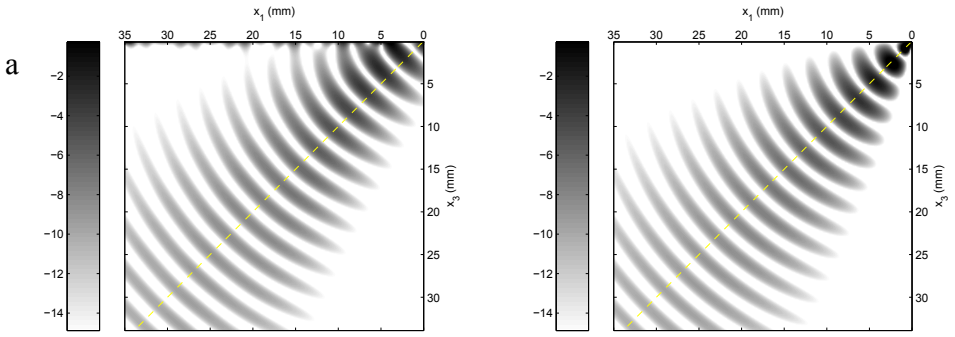

Figure 13: Displacement beneath a P probe for a fix frequency, with numerical quadrature (a) and stationary phase (b)

Investigations by Liu and Wirdelius [2006] shows that the probe model generates a displacement field that behaves as a plane wave in the far field. For this reason, each ray

is locally treated as a plane wave. The amplitude of each ray, representing a perpendicular wave front, is in 2 dimensions decaying as the square rot to the distance.

The weld model

The model of the weld is based on a relatively primitive assumption of the grain structure for a V-butt weld. The columnar structure of austenitic welds is here modelled as a weld where each sub region corresponds to a grain group, figure 14. Each grain group is characterized as an homogeneous, transversely isotropic region. The weld then shows a highly anisotropic behaviour.

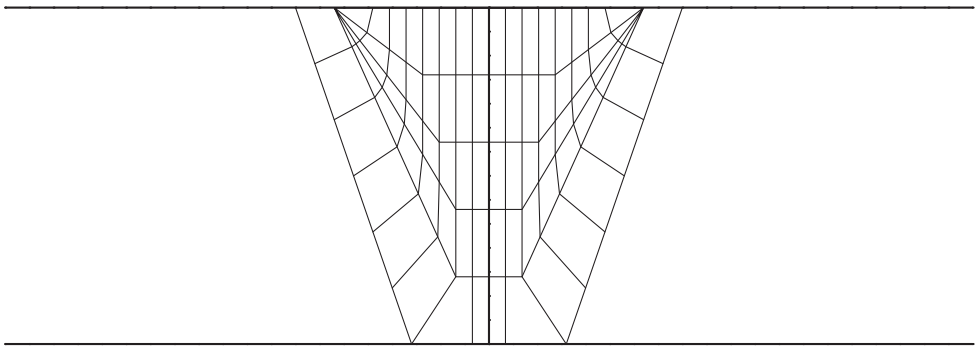

Figure 14: Model of a V-butt, showing sub regions

The justification for the weld model is provided in Liu and Wirdelius [2006] and the previous macroscopic study of the solidification structure of the addressed welds. The five constants $C_{11}, C_{12}, C_{13}, C_{33}, C_{44}$ that describes the weld material as transversely anisotropic were measured and then compared with analytical calculations according to the model by Voigts. The stiffness matrix is

$$\mathbf{C}_{ij} = \begin{bmatrix} C_{11} & C_{12} & C_{13} & 0 & 0 & 0 \\ C_{12} & C_{11} & C_{13} & 0 & 0 & 0 \\ C_{13} & C_{13} & C_{33} & 0 & 0 & 0 \\ 0 & 0 & 0 & C_{44} & 0 & 0 \\ 0 & 0 & 0 & 0 & C_{44} & 0 \\ 0 & 0 & 0 & 0 & 0 & C_{66} \end{bmatrix}$$

where $C_{66} = \dfrac{C_{11} - C_{12}}{2}$

The investigation showed a good agreement between the measurements and the calculations. These constants for the transversely anisotropic material are used in the different regions of the weld model with an orientation according to the dendrite structure.

The region outside the weld is assumed to have homogeneous isotropic elastic properties.

The ray tracing

The ray tracing technique is based on geometrical optics and a 2D algorithm that has been developed (see Liu et. al. [2007]). For the high frequencies considered, the ultrasound trajectory is treated as a ray. In this asymptotic approach the solution to Helmholtz equation is written as

$$\psi^P = e^{\mathrm{i}k_P\varphi_P(\mathbf{x})}\sum_{n=0}^{\infty}\frac{A_n^P(\mathbf{x})}{(\mathrm{i}k_P)^{n+1}}$$

$\varphi_P(\mathbf{x})$ is the phase function and $A_n^P(\mathbf{x})$ is the amplitude in the nth order of approximation. Using only the first term in the series ($n = 0$) $\varphi_P(\mathbf{x})$ defines the wavefront. For an isotropic medium this is the wave vector direction and the energy propagating direction. The anisotropic case is more complicated and here the ray direction is derived from this relationship between phase and group velocity.

Here this model has been extended to include rays reflected in the back surface, including reflection inside the weld. In the far-field, as is the case in this study, these rays are representing plane waves.

The signal response

The practical ultrasonic testing is understood to be made with a transmitter-receiver in a tandem configuration. The response of the receiver is here calculated according to Auld's reciprocity principle, that is: the calculated signal response $\delta\Pi$ is the change in the electrical transmission coefficient due to the scatterer.

Denote by V the output observed when a signal is transmitted from the transmitter to the receiver in the presence of a scatterer (the weld and the back surface). In the time domain V can be calculated as

$$V = \frac{1}{2\pi}\int_{-\infty}^{\infty}\delta\Pi\,\tilde{f}e^{-i\omega t}dw = \delta\Pi * f$$

where * denotes time convolution, $\delta\Pi$ is the signal response, $\tilde{f}$ is the frequency spectrum in the frequency domain of the input signal. The frequency spectrum of the input signal in the time domain is denoted f.

Using reciprocity arguments according to Auld [1979] the signal response $\delta\Pi$ can be calculated as

$$\delta\Pi = -\frac{i\omega}{4P}\int_{\Gamma}(\boldsymbol{u}_2\cdot\boldsymbol{t}_1 - \boldsymbol{u}_1\cdot\boldsymbol{t}_2)\,d\Gamma$$

Here Γ denotes the border of the closed integration contour, P the probe effect and ω the fixed frequency. The displacement $\boldsymbol{u}_1$ and the traction $\boldsymbol{t}_1$ belongs to state 1 and $\boldsymbol{u}_2$, $\boldsymbol{t}_2$ to state 2. Here state 1 is chosen as the solution when the probe is transmitting in the presence of the scatterer, that is the actual testing situation where the transmitter is working as a transmitter, and the integration contour chosen to include the weld and the back surface, see figure 15. The integration contour follows the boarder of the weld and the back surface, enclosing both the weld and the back surface inside the contour with inward directed normal.

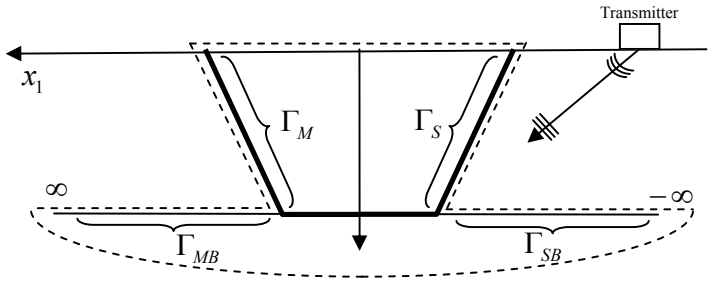

Figure 15: State 1

State 2 is the solution when the probe is transmitting in the absence of the scatterer, the receiver is acting as a transmitter and the integration contour corresponds to the one in state 1. In state 2 there is no weld and no back surface present, see figure 16, but the displacement $\boldsymbol{u}_2$ and traction $\boldsymbol{t}_2$ is calculated on the same boarder as in state 1.

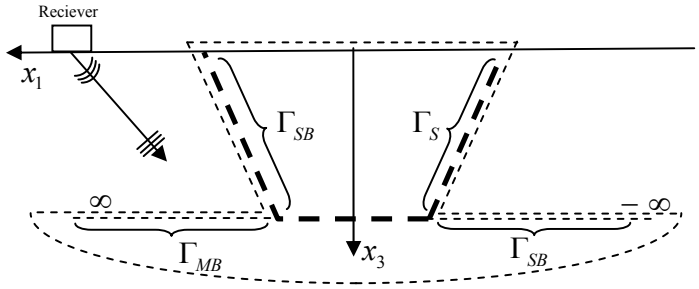

Figure 16: State 2

Since the boarder of the weld for $x_3 = 0$ is traction free in both state 1 and state 2 this part of the integration contour will give no contribution. The border Γ_{SB} and Γ_{MB} is also free of traction in state 1 but not in state 2.

The model of the weld can treat an anisotropic weld in an isotropic media. Calculations in this study are made on the boarder of the weld or in the isotropic media, although the ray tracing inside the weld is made for an anisotropic media.

UT data collection

UT data collection was performed by SQC according to guidelines given from Chalmers. The purpose to collect data from real inspection objects with known material structure is to compare experimental data with theoretically calculated values.

Data has been collected from four different test blocks called A18, B27, C20 and D20, see figure 17. Data from 64 different combinations of material, wave modes, and angle of refractions and positions of probe relative the weld has been collected. Data was collected during year 2005 in SQC facilities, Täby Stockholm.

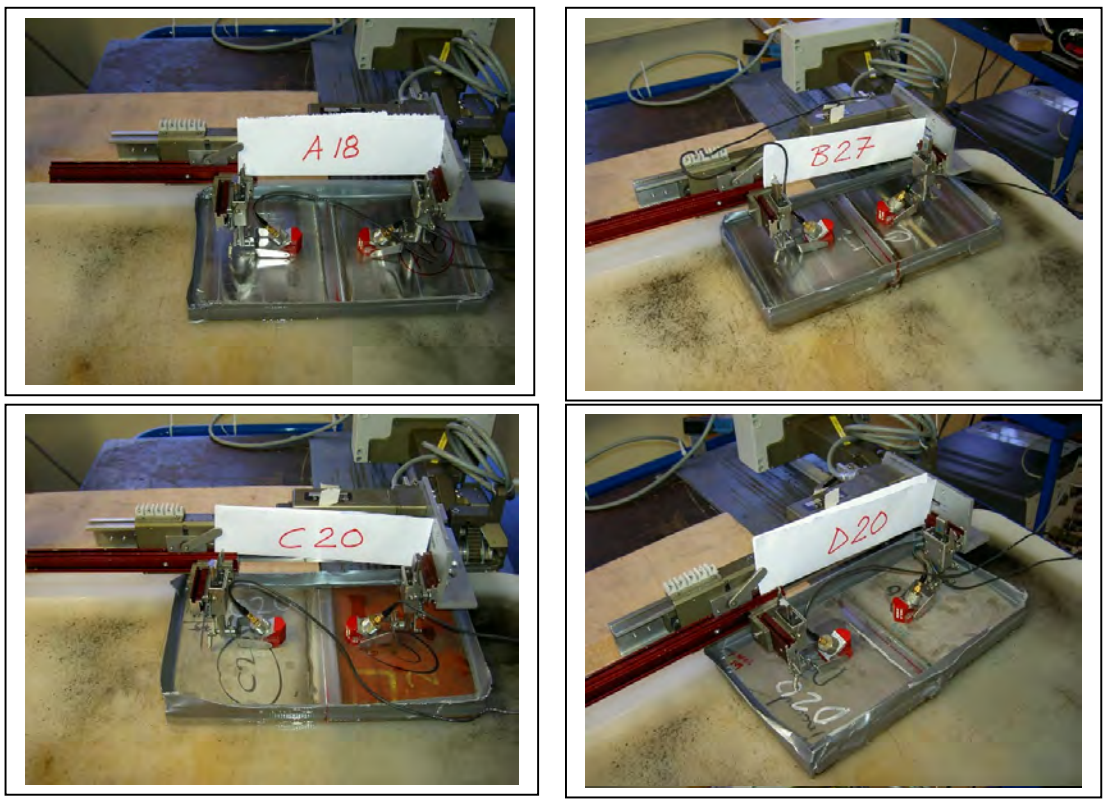

Figure 17: Test bocks A18, B27, C20 and D20.

Test blocks

The test blocks were manufactured in an earlier partial project, UliAS task 2 [1999]. The test blocks represent four different material combinations. A18 and B27 are plates with

base material of austenitic stainless steel welded together with an austenitic stainless steel weld. C20 has base material of stainless steel on one side and carbon steel on the other side and is welded together with Inconel 82/182. Finally the D20 test block identically with C20 but has the carbon steel side replaced by Inconel 600. In table 1 more details are given regarding the test blocks.

Test block	Thickness (mm)	Base material plate 1	Base material plate 2	Welding material
A18	18	X5CrNi189 (AISI 304)	X5CrNi189 (AISI 304)	X1CrNi19-9 (AISI 308L)
B27	27	X10CrNiNb189 (AISI 347)	X10CrNiNb189 (AISI 347)	X1CrNi19-9 (AISI 308L)
B20	20	X5CrNi189 (AISI 304)	19Mn6 (CS)	Inconel 82/182
C20	20	X5CrNi189 (AISI 304)	Inconel 600	Inconel 82/182

Table 1: Test blocks – Material and dimensions.

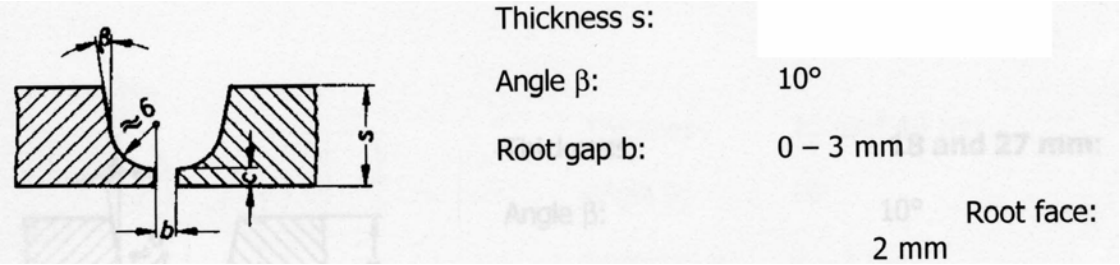

Figure 18: Groove angle

Welding specifications are described in figure 18. Macro pictures from the test blocks is indicating the following values for; b=2 mm for A18 and b =1 mm for the other three.

Experimental setup

Collection of data has been performed by keeping one probe on a fixed distance see Table 2) from the weld centre line and scans the other probe perpendicular to the weld in line with the other probe. This has been repeated for a length of 50 mm along the weld and with an increment of 4 mm and for four different positions of the fixed probe. For some cases the increment has been set to 2 mm. See also figure 19.

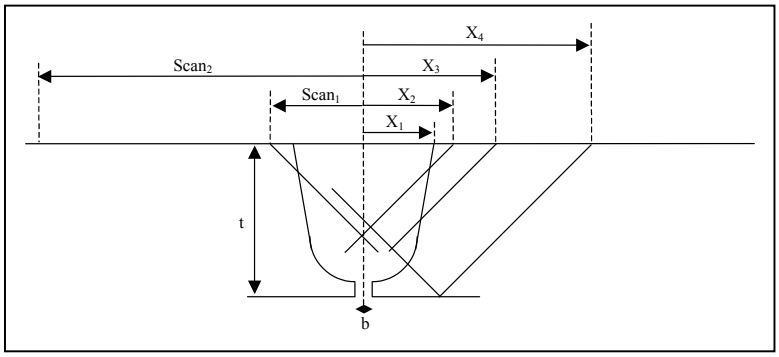

Figure 19: Principle for 45° probe.

In table 3-4, all experimental setups are presented.

Case	**x_1**	**x_2**	**x_3**	**x_4**	**$scan_1$**	**$scan_2$**
A18-45°	9	12	16	24	12	48
B27-45°	10	18	24	36	14	68
C20-45°	9	13	18	27	12	52
D20-45°	9	13	18	27	12	52
A18-60°	9	12	22	45	12	82
B27-60°	10	18	33	67	14	108
C20-60°	9	13	24	50	12	82
D20-60°	9	13	24	50	12	82

Table 2: Scanned areas.

Plate	**A18**				**B27**				**C20**				**D20**			
Probe distance weld centre line	9	12	16	24	10	18	24	36	9	13	18	27	9	13	18	27
Probe																
45 shear 1 MHz	X	X	X	X	X	X	X	X	X	X	X	X	X	X	X	X
45 shear 2,25 MHz	X	X	X	X	X	X	X	X	X	X	X	X	X	X	X	X

Table 3: Probe 45°.

Plate	A18				B27				C20				D20			
Probe distance weld centre line	9	12	22	45	10	18	33	67	9	13	24	50	9	13	24	50
Probe																
60 shear 1 MHz	X	X	X	X	X	X	X	X	X	X	X	X	X	X	X	X
60 long 1 MHz	-	-	-	-	X	X	X	X	-	-	-	-	-	-	-	-

Table 4: Probe 60°l.

For test block D20 and C20 where the base material is not the same on both sides of the weld the fixed probe has been place on the carbon steel side respectively Inconel 600 side.

Equipment and probes

Instrument: Tomo SV RD Tech

Soft ware: Data acquisition RD Tech 1.3B3
Evaluation Zetec Ultra Vision 1.0R5

Probes: Panametric V-series. Crystal size Ø 13 mm 1,0 och 2,25 MHz, wedge 45º and 60º longitudinal respectively shearwave. Model V-series are probes that are broad banded.

In this investigation the sensitivity is more or less unimportant. The sensitivity should only be set to a value close to a saturated signal.

Manipulator

Manipulator: AWS-6, Force Technology

Motor control: Phoenix PC-Link MCPA2-2

Personnel

Jeanette Gustafsson UT level 2

Kjell Högberg UT level 3

Evaluation of data

For each case three positions (x-values) has been evaluated. The y-position for maximum amplitude together with the sound path are recorded. The following x –values has been used 71,7 or 72 mm, 55 or 56 mm and 38,3 or 38 mm. For those cases where data has been of bad quality adjacent x-positions has been used. If the signal is too much saturated (>100%) the recording is less precise. This has been indicated with brackets around the x –value in the tables. Figure 20 explains the information on the printouts in appendices 1-13and in table 5 there are a summary of the appendices.

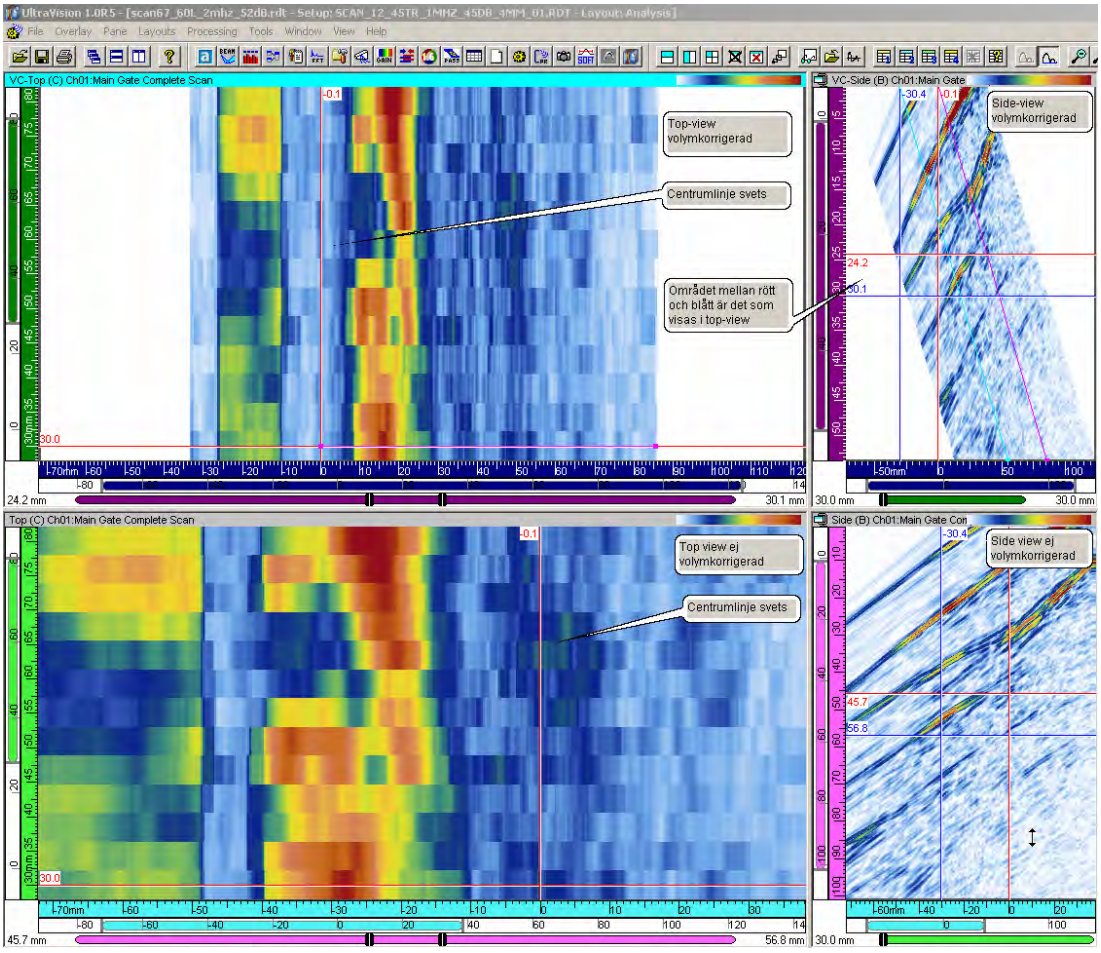

Figure 20: Example print-out, 60° longitudinal. The upper picture is volume corrected and the lower one without. The red vertical line represents the weld centre line. The area between the horizontal red and blue line are presented in the top view.

PLate	**A18**				**B27**				**C20**				**D20**			
Probe distance weld centre line	9	12	16	24	10	18	24	36	9	13	18	27	9	13	18	27
Probe																
45 shear 1 MHz	1:1	1:2	1:3	1:4	2:1	2:2	2:3	2:4	3:1	3:2	3:3	3:4	4:1	4:2	4:3	4:4
45 shear 2,25 MHz	5:1	5:2	5:3	5:4	6:1	6:2	6:3	6:4	7:1	7:2	7:3	7:4	8:1	8:2	8:3	8:4
Plate	**A18**				**B27**				**C20**				**D20**			
Probe distance weld centre line	9	12	22	45	10	18	33	67	9	13	24	50	9	13	24	50
Probe																
60 shear 1 MHz	9:1	9:2	9:3	9:4	10:1	10:2	10:3	10:4	11:1	11:2	11:3	11:4	12:1	12:2	12:3	12:4
60 long 1 MHz	-	-	-	-	13:1	13.2	13:3	13:4	-	-	-	-	-	-	-	-

Table 5: Reference to figures in appendix 1, example 1:2 is enclosure 1 figure 2.

Simulation results

The results from the simulations are presented in appendix 2 and follow the UT data collection scheme presented in table 5. Though the situation with the transmitter close to the weld is excluded since the approximation, done by using ray tracing, only is valid in the far field of the transmitter. The probe is represented by seven rays that are distributed evenly between ±6° from the nominal angle of modelled transmitter. This angle represents the main lobe of the generated and received field (see Liu et. al. [2007]). In figure 21 an example of produced results is presented. The upper picture visualizes the ray tracing through the sub regions and does not include any information of amplitude distribution. In the middle plot the level of received amplitude from a line scan is depicted and the lowest is a C-scan produced by eight identical line scans.

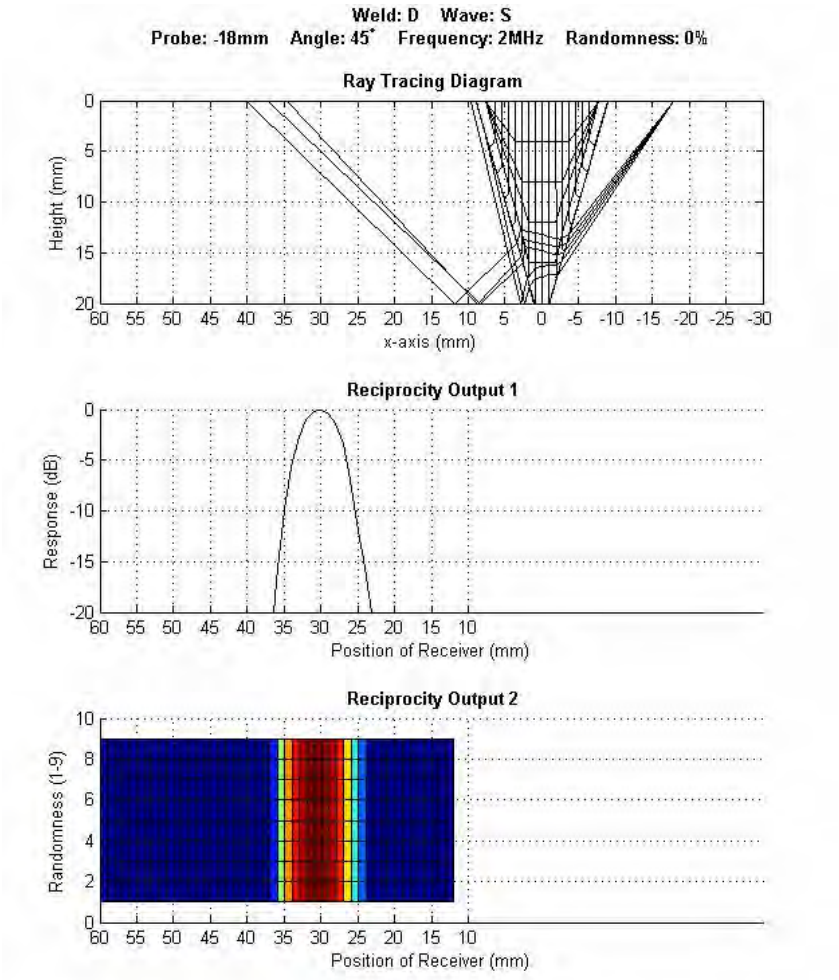

Figure 21: The output generated by the simulation software. The ray tracing is depicted in the upper figure while the received signal response, as function of receiver position, are plotted in the lower ones.

One interesting observation from figure 21 is that the ad hoc assumption made from the upper picture that the maximum response should be found in one region that isn't correlated to the actual maximum from experiments and simulated line scans. This is assumed to be caused by the fact that the amplitude of the received signal response is imposed by four major components: the divergence of the probe when it is acting as transmitter, the divergence of the probe when it is acting as receiver, the spread caused by the weld and the angle dependency of the reflection coefficient (back wall).

From the experimental result it is obvious that the anistropic behaviour varies along the welding direction. Some of these variations are caused by variation in other parameters such as surface conditions and couplant conditions but not all variations can be explained by these. This variation is assumed to be caused by variation in the orientation of the dendrites. These variations can not be modelled as such by the mathematical model since it assumes a two dimensionality. In order to validate the degree of variation a number of simulations of the same situation was generated with a random variation of the dendrite orientation. These were then combined into a C-scan which made it possible to make a qualitative comparison with the experimental data (see appendix 1). Note that the experimental C-scans were corollary built up with a number of line scans. The randomisation was limited to a percentage in increment from the original orientation and the best correlation in all simulations, both hence weld type and used probe, was a 5% variation (see figure 22 and 23).

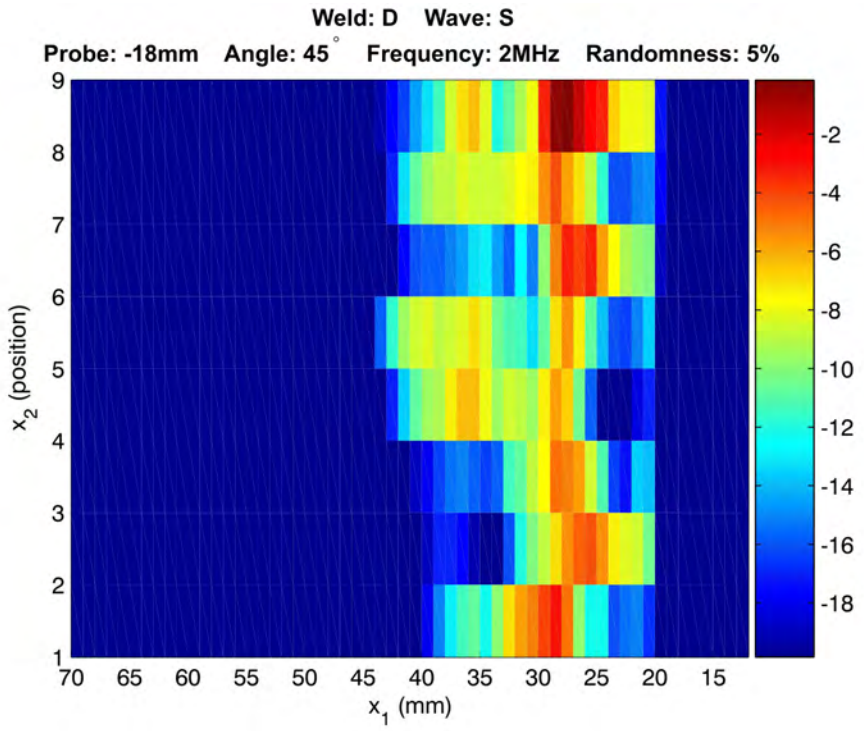

Figure 22: The simulated C-scan that corresponds to figure 21.
It is built by 8 line scan simulations with 5% of randomized variation of the denrite orientation within each sub region(see figure 14).

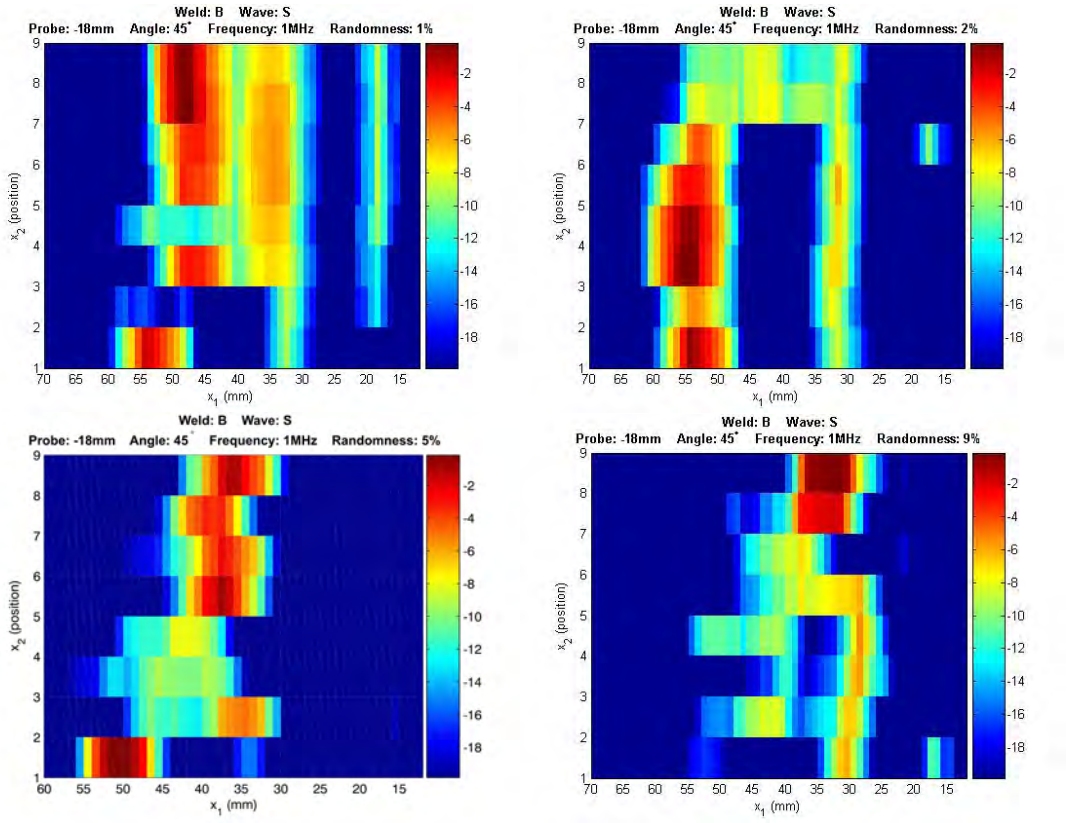

Figure 23: The simulated C-scan that corresponds to figure 21. It is built by 8 line scan simulations with percentage (1,2,5,and 9%) of randomized variation of the dendrite orientation within each sub region(see figure 14).

All simulations corresponding to the experimental data in appendix 1 are documented in appendix 2 and depicted in table 6. Note that all simulations have been non-quantitative in such sense that each maximum has been forced into 1 and used as calibration, i.e. all other values in the C-scan have been divided with this value. This since it was the distribution of energy that was of interest and therefore no model of damping was included.

Plate	**A18**				**B27**				**C20**				**D20**			
Probe distance weld centre line	9	12	16	24	10	18	24	36	9	13	18	27	9	13	18	27
Probe																
45 shear 1 MHz																
Page	-	1	1	2	-	2	3	3	-	4	4	5	-	5	6	6
45 shear 2,25 MHz																
Page	-	7	7	8	-	8	9	9	-	10	10	11	-	11	12	12
Plate	**A18**				**B27**				**C20**				**D20**			
Probe distance weld centre line	9	12	22	45	10	18	33	67	9	13	24	50	9	13	24	50
Probe																
60 shear 1 MHz																
Page	-	13	13	14	-	14	15	15	-	16	16	17	-	17	18	18
60 long 1 MHz																
Page	-	-	-	-	-	19	19	20	-	-	-	-	-	-	-	-

Table 6: Reference to simulations correlating to table 5 that are included in appendix 2.

Concluding remarks

A two dimensional mathematical model of a specific ultrasonic NDT situation has been modelled and validated together with experimental data. The NDT situation has been chosen in order to detect wave propagation through an anisotropic weld. The experimental phases revealed that the assumed two dimensionality of the weld was not sufficient in order to make a realistic match. In order to quantify this anomalies a number of line-scans with individual randomised variation of transversal anisotropic behaviour was summarised into a C-scan. The randomisation was limited to a percentage in increment from the original orientation. The best correlation in all simulations, both hence weld type and used probe, was a 5% variation. The cause of this variation in texture has been documented in Aronsson, P. and Söderman (1995) and can be minimised by mechanised welding and other welding methods (e.g. laser- or frit steer welding).

The outcome of the project documented in this paper will be to use the forward model in an optimising scheme. The quantification of variation will be used to limit down the variation each sub volume can be given. This is essential when the global solver is addressing the invert problem and the solution to the inverse problem would take enormous capacity in computer power and time. The basic idea is to develop a NDT method using ultrasonic conventional probes in order to sample enough information about the weld in order to calculate the texture (i.e. the dendrite orientation) in the weld. This information is thereafter used to implement in software that models the NDT situation including a defect. In this way the information enables a realistic simulation of the actual simulation problem.

References

Aronsson, P. and Söderman, L., SKI Report 95:75, Stockholm (1995).

Auld, B.A., *General Electromechanical Reciprocity Relations Applied to the Calculation of Elastic Wave Scattering*, Wave Motion, vol. 1, 1979, pp. 3-10.

Boström, A., *Ultrasonic Benchmarking with UTDefect*, Review of Quantitative Nondestructive Evaluation, Thompson, D.O. and Chimenti, D.E., eds., vol. 24, American Institute of Physics, 2005, pp. 1859-1863.

Collet, N. J. & Hawker, B., "Measurement of elastic constants for Inconel 182 weld material", Int. Comm. , IVC/RTID/MOD/RAY-1, Culham (1998).

Diligent, O., Chatillon, S., Lhémery, A., and Mahaut, S., *Results of the 2004 UT Modeling Benchmark Obtained with the CIVA Software Developed at the CEA*, Review of Quantitative Nondestructive Evaluation, Thompson, D.O. and Chimenti, D.E., eds., vol. 24, American Institute of Physics, 2005, pp. 1843-1850.

Eriksson, A., *Ultraljudsegenskaper i austenitiska svetsar; Slutrapport*, TRC Rapport R-T98-03, Täby (1998).

Halkjaer, S, *Ultrasonic parameters in autenitic weldings; ULiAS task 2 progress report 3*, FORCE Report 3 PF4099-119077, (2000).

Lakestani, F., *Validation of mathematical models of ultrasonic inspection of steel components*, PISC III Report 16, JRC, Inst. Adv. Mat., Petten, The Netherlands, 1992.

Liu, Q. and Wirdelius, H., *A 2D model of ultrasonic wave propagation in an anisotropic weld*, NDT & E international, 2006, vol 40, pp 229-238.

Liu, Q., Persson, G. and Wirdelius, H., *A receiver model for the ultrasonic ray tracing simulation on an anisotropic weld*, submitted for publication, 2007.

Nielsen, S.A., *Ultrasonic parameters in autenitic weldings; ULiAS task 2 progress report 2,* FORCE Final Report PF4099-119077, (1999).

Nielsen, S.A., *Ultrasonic parameters in autenitic weldings; ULiAS task 3 final report* ,FORCE Final Report 170760, (2000).

Nielsen S. A., *Ultrasonic Parameters in Austenitic Weldings UliAS Task 3, Appendices for Final Report*, Force Technology, 31 October 2002.

Schmerr Jr., L.W., Kim, H.-J., Lopez, A.L., and Sedov, A., *Simulating the Experiments of the 2004 Ultrasonic Benchmark Study*, Review of Quantitative Nondestructive

Evaluation, Thompson , D.O. and Chimenti, D.E., eds., vol. 24, American Institute of Physics, 2005, pp. 1880-1887.

Song, S.-J., Park, J.-S., Choi, Y.-H., Kang, S.-C., and Kim, K.-J., *Model Predictions to the 2004 Ultrasonic Benchmark Problems*, Review of Quantitative Nondestructive Evaluation, Thompson, D.O. and Chimenti, D.E., eds., vol. 24, American Institute of Physics, 2005, pp. 1872-1879.

Spies, M., *Prediction of Ultrasonic Flaw Signals and Model-to-Experiment Comparison*, Review of Quantitative Nondestructive Evaluation, Thompson, D.O. and Chimenti, D.E., eds., vol. 24, American Institute of Physics, 2005, pp. 1851-1858.

Söderman, L., *Ultraljudsegenskaper i austenitiska svetsar; Del 1.1 Litteraturstudie*, TRC Rapport R-T97-88, Täby (1997).

Österberg, E., *Ultraljudsegenskaper i austenitiska svetsar; Del 1.2 Inventering av objekt*, TRC Rapport R-T97-108, Täby (1997).

Österberg, E., *Ultraljudsegenskaper i austenitiska svetsar; Del 1.3 Specifikation av studier*, TRC Rapport R-T97-113, Täby (1997).

www.ski.se

STATENS KÄRNKRAFTINSPEKTION
Swedish Nuclear Power Inspectorate

POST/POSTAL ADDRESS SE-106 58 Stockholm
BESÖK/OFFICE Klarabergsviadukten 90
TELEFON/TELEPHONE +46 (0)8 698 84 00
TELEFAX +46 (0)8 661 90 86
E-POST/E-MAIL ski@ski.se
WEBBPLATS/WEB SITE www.ski.se